

Published by ASME. Commercial use only.

© 2024 The American Society of Mechanical Engineers

Access to this work was provided by the University of Maryland, Baltimore County (UMBC) ScholarWorks@UMBC digital repository on the Maryland Shared Open Access (MD-SOAR) platform.

**Please provide feedback**

Please support the ScholarWorks@UMBC repository by emailing [scholarworks-group@umbc.edu](mailto:scholarworks-group@umbc.edu) and telling us what having access to this work means to you and why it's important to you. Thank you.

**W. J. Birmingham<sup>1</sup>**

Dusty Plasma Laboratory,  
Mechanical Engineering Department,  
University of Maryland Baltimore County,  
Baltimore, MD 21250  
e-mail: birming2@umbc.edu

**E. M. Bates<sup>1</sup>**

Dusty Plasma Laboratory,  
Mechanical Engineering Department,  
University of Maryland Baltimore County,  
Baltimore, MD 21250  
e-mail: evbates1@umbc.edu

**C. A. Romero-Talamás**

Dusty Plasma Laboratory,  
Mechanical Engineering Department,  
University of Maryland Baltimore County,  
Baltimore, MD 21250  
e-mail: romero@umbc.edu

# Analytic Thermal Design of Bitter-Type Solenoids

*We describe an analytic approach to designing axially water-cooled Bitter-type electromagnets with an emphasis on heat dissipation considerations. The design method here described aims to enhance the efficiency of the design process by minimizing the role of finite element analysis (FEA) software. A purely analytic design optimization scheme is prescribed for establishing the cooling hole placement. FEA software is only used to check the accuracy of analytic predictions. The analytic method derived in this paper predicts the required heat dissipation rate by approximating the volumetric joule heating profile with a smooth, continuous profile. Equations for turbulent convective heat transfer in circular ducts are generalized to model the cooling capacity of elongated cooling passages. This method is currently in use at the University of Maryland Baltimore County Dusty Plasma Laboratory to design a Bitter magnet capable of generating fields of 10 T. [DOI: 10.1115/1.4031888]*

## 1 Introduction

In recent decades, FEA software has become an invaluable tool in Bitter magnet design [1]. FEA is a highly effective method for visualizing and quantifying gradients and parameters in complex systems; however, such software is costly and often requires extended computation time. Particularly in the initial stages of the design process, such constraints can greatly inhibit design exploration and optimization. Thus, the use of analytic expressions early in the design phase can greatly enhance the efficiency and efficacy of the magnet design process.

In the infancy of Bitter magnet technology and prior to the advent of FEA, Brechna and Montgomery [2], Bitter [3], and others formulated expressions for understanding the performance of resistive magnets. Today, the design of Bitter magnets has evolved considerably, and analytic methods have been updated to accommodate modern design concepts [4]. However, a clear presentation of analytic thermal design methodology has not been published, since more advanced cooling designs were discovered. We present a method for designing Bitter magnet cooling systems, which applies to modern elongated cooling channels and which does not rely heavily on FEA. Additionally, the expressions derived in this analysis, unlike those determined by older empirical analyses, can be generalized to evaluate hitherto unexplored design concepts.

The magnet design process herein described is being utilized by the Dusty Plasma Laboratory at the University of Maryland Baltimore County. We are seeking to analyze magnetized dusty plasma in fields of 10 T. Figure 1 shows a preliminary design currently under consideration.

## 2 General Design Considerations

The method adopted here for Bitter magnet design is as follows. First, the electromagnetic optimization is completed to establish the requisite size, electrical current, and power dissipation. Second, thermal calculations are used to define the approximate

cooling channel design. Finally, mechanical stress due to the Lorentz force is taken into account, and the overall design as well as the location of the support struts are modified accordingly. The heat dissipation requirements must be evaluated after electromagnetic calculations because the joule heating depends on the power that is required to obtain the desired field. The mechanical stress calculations are completed last because the stress concentrations are mainly determined by the geometry and placement of the cooling passages. These steps can then be repeated several times until the design converges to an optimized solution. This analysis will primarily consider the second-stage of this design sequence.

The most often used cooling system for Bitter-type solenoids consists of axially oriented cooling passages through which chilled deionized water is run. Determination of the location and

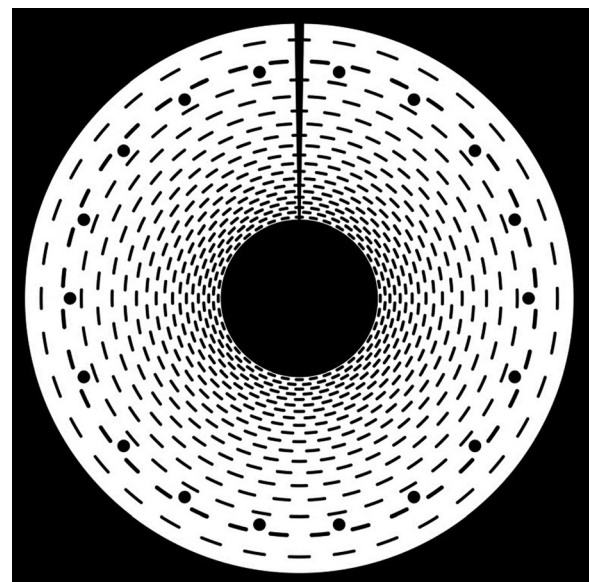


**Fig. 1 Example cooling hole pattern currently under consideration. The bore diameter is 16 cm and the outer diameter is 55.9 cm.**

<sup>1</sup>Corresponding author.

Contributed by the Heat Transfer Division of ASME for publication in the JOURNAL OF THERMAL SCIENCE AND ENGINEERING APPLICATIONS. Manuscript received March 2, 2015; final manuscript received October 9, 2015; published online December 4, 2015. Assoc. Editor: Giulio Lorenzini.



Fig. 2 Elongated (left) and circular (right) cooling channels

size of these cooling passages is by far the greatest challenge in heat management. To ensure the safety and functionality of the apparatus, the cooling passages must provide sufficient surface area for heat dissipation without compromising the strength of the structure.

### 3 Joule Heating Profile

To design the cooling system, it is first necessary to obtain an expression that can accurately predict the joule (or ohmic) heating profile within the magnet. The following derivation follows the same methodology which Brechna and Montgomery used to obtain expressions for circular cooling channels [2]. More recent research has determined that in fact elongated and staggered cooling channels (see Fig. 2) allow for better thermal management and structural support [5]. The equation obtained below yields the joule heating profiles for coils with these elongated passages and shows agreement with FEA.

The equation for current density in a disk-shaped solenoid (with no cooling passages) as a function of radius,  $r$ , from the center axis is given by [6]

$$j(r) = j_0 \left( \frac{a_1}{r} \right) \quad (1)$$

where  $a_1$  is the inner coil radius, and  $j_0$  is the current density at  $a_1$ . The volumetric joule (or ohmic) heating as a function of current density is

$$w_v = \rho j^2 \quad (2)$$

where  $\rho$  is the resistivity. Thus, for a disk-type solenoid, volumetric joule heating at some radius,  $r$ , is

$$w_v(r) = \rho j_0^2 \left( \frac{a_1}{r} \right)^2 \quad (3)$$

This expression can now be integrated over the entire volume of the coil to obtain the total heat generated due to resistive losses. However, this presents a problem, for the heat generation predictions are intended to serve as a design aid. Hence, at the design phase in which heating profile predictions are most useful, the geometry of the cooling channel system has not yet been determined. For this reason, it is necessary to formulate an expression that is a function of bulk design parameters. The bulk parameters which define the heating profile derived below include the total number of cooling channel rings, the number of magnetic turns, the width of the cooling channels, and the overall dimensions of the coil. After an initial approximate cooling system has been designed, the bulk parameters can be modified accordingly in a second iteration.

To derive the expression, we define a variable,  $\lambda_r$ , which represents the fill factor due to cooling channels as a function of the radius. This fill factor or density factor gives the fraction of the

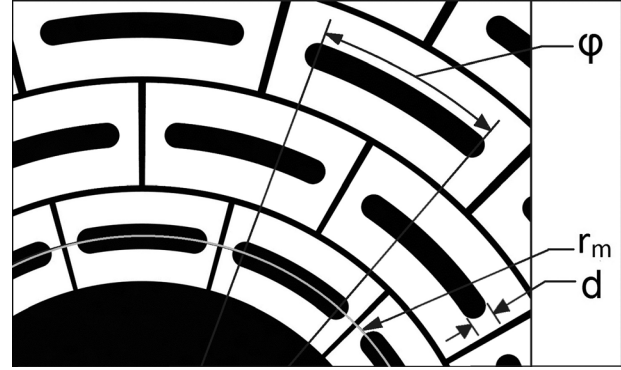


Fig. 3 Polar lattice divisions with cooling channel ring locations defined by  $r_m$

total disk area that is composed of electrically conductive material. Because the joule heating varies inversely with  $r^2$ , the heat generation is much higher near the inner bore of the coil. This requires that the cooling hole pattern be much tighter in this region. Thus, the tightness of the cooling hole pattern varies with radius. In order to accurately represent the geometry and accurately predict the joule heating, it is necessary that the fill factor varies with radius as well.

The surface of the coil can be divided into a lattice of polar rectangles with a cooling channel in the center of each (as shown in Fig. 3). The radial position of the center of a given cooling channel (and thus the center of the polar rectangle) is denoted  $r_m$ . The height (radial extent) of each polar rectangle is the total radial extent of the disk,  $(a_2 - a_1)$ , divided by the number of cooling channel layers (or rings),  $N_R$ . The width (circumferential extent) is the circumference corresponding to the radius,  $r_m$ , divided by the number of holes per ring,  $n$ . And so, the area of a rectangle at some radius,  $r_m$ , is given by

$$A_r = \int_0^{2\pi} \int_{r_m - \frac{a_2 - a_1}{2N_R}}^{r_m + \frac{a_2 - a_1}{2N_R}} r dr d\theta = \frac{2\pi r_m (a_2 - a_1)}{n N_R} \quad (4)$$

where  $a_2$  is the outer radius of the coil. There is one cooling channel per rectangle, thus, the expression for holes per unit area,  $m$ , is given by

$$m = \frac{1}{A_r} = \frac{n N_R}{2\pi r_m (a_2 - a_1)} \quad (5)$$

The area of one elongated cooling hole at some radius,  $r_m$ , with some radial thickness,  $d$ , and which spans some angle between the semicircular ends,  $\phi$  (in radians), is given by

$$A_h = \frac{\pi d^2}{4} + \phi r_m d \quad (6)$$

Thus, the fill factor due to cooling holes is given by

$$\begin{aligned} \lambda_r(r_m) &= 1 - mA_h \\ &= 1 - \frac{n N_R}{8 r_m (a_2 - a_1)} \left( d^2 + \frac{4}{\pi} \phi r_m d \right) \end{aligned} \quad (7)$$

This expression yields the fill factor at each rectangle, but in order to integrate over the entire coil, the above expression must be a continuous function of  $r$ , not a stepwise function of  $r_m$ .

It is important to note at this point that it is advantageous to make dense cooling hole patterns in Bitter coils. This principle has been established by other Bitter magnet designers [7], and we

have found this to be true empirically after several design studies. A temperature gradient arises between adjacent cooling passages such that increasing the distance between channels increases the resultant peak temperature. Because of this, we have found that, for Bitter magnets with tight cooling hole patterns, accurate joule heating predictions can be obtained if the volume of the coil is approximated by applying Eq. (7) continuously over the disk space. That is,  $\lambda_r(r_m)$  becomes  $\lambda_r(r)$ . The expression for  $\lambda_r(r)$  can now be used to obtain the total joule heating,  $W$ , for the entire volume of the solenoid

$$dW = w_v(r) \lambda_r(r) dV \quad (8)$$

$$W = \int_0^{N_T \alpha_T t} \int_0^{2\pi} \int_{a_1}^{a_2} w_v(r) \lambda_r(r) r dr d\theta dz \quad (9)$$

where  $N_T$  is the number of magnetic turns,  $\alpha_T$  is the number of Bitter disks per turn, and  $t$  is the thickness of a Bitter disk. (Thus,  $N_T \alpha_T t$  is the effective height of the copper stack with the insulators removed.) Inserting Eqs. (3) and (7) into the above expression, we obtain

$$\begin{aligned} W &= \int_0^{N_T \alpha_T t} \int_0^{2\pi} \int_{a_1}^{a_2} \rho j_0^2 \left( \frac{a_1}{r} \right)^2 \\ &\quad \times \left( 1 - \frac{n N_R}{8 r (a_2 - a_1)} \left( d^2 + \frac{4}{\pi} \phi r d \right) \right) r dr d\theta dz \\ &= 2\pi \rho j_0^2 a_1^2 N_T \alpha_T t \left[ \left( 1 - \frac{n N_R d \phi}{2\pi (a_2 - a_1)} \right) \ln \left( \frac{a_2}{a_1} \right) - \frac{n N_R d^2}{8 a_2 a_1} \right] \end{aligned} \quad (10)$$

This equation can now be used to derive a more useful expression for volumetric joule heating. Solving Eq. (3) for  $\rho(j_0 a_1)^2$ , inserting it into Eq. (10), and then solving for  $w_v$ , yields

$$w_v(r) = \frac{W}{2\pi N_T \alpha_T t \left[ \left( 1 - \frac{n N_R d \phi}{2\pi (a_2 - a_1)} \right) \ln \left( \frac{a_2}{a_1} \right) - \frac{n N_R d^2}{8 a_2 a_1} \right]} \frac{1}{r^2} \quad (11)$$

This expression compared with an FEA model shows close agreement, as seen in Figs. 4 and 5. The cooling hole pattern shown in Fig. 1 is used as a case study. Figure 4 reveals that for a radial line element which spans a total of ten cooling channels

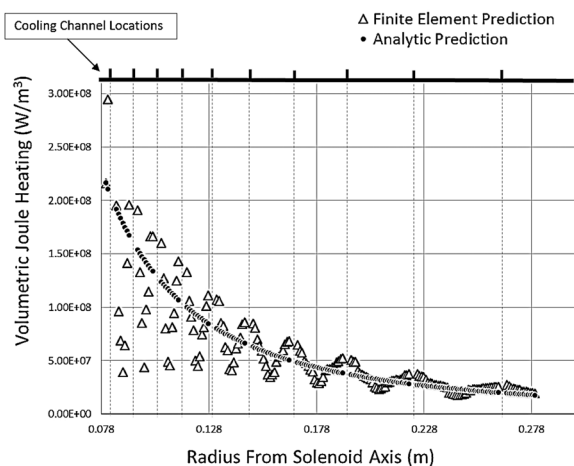


Fig. 4 Joule heating profile predictions for a copper coil given 4200 A-10 hole path

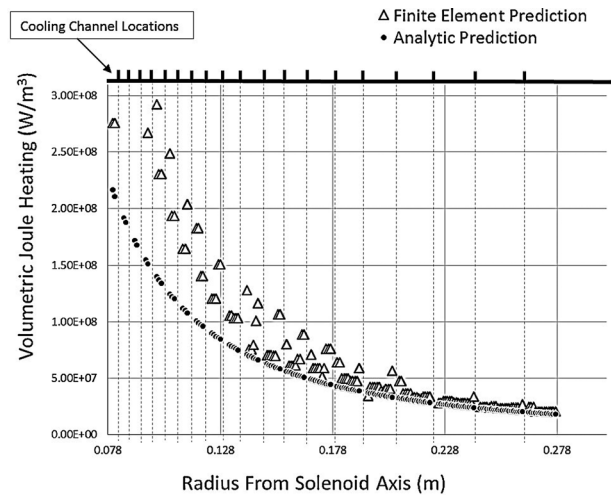


Fig. 5 Joule heating profile predictions for a copper coil given 4200 A-19 hole path

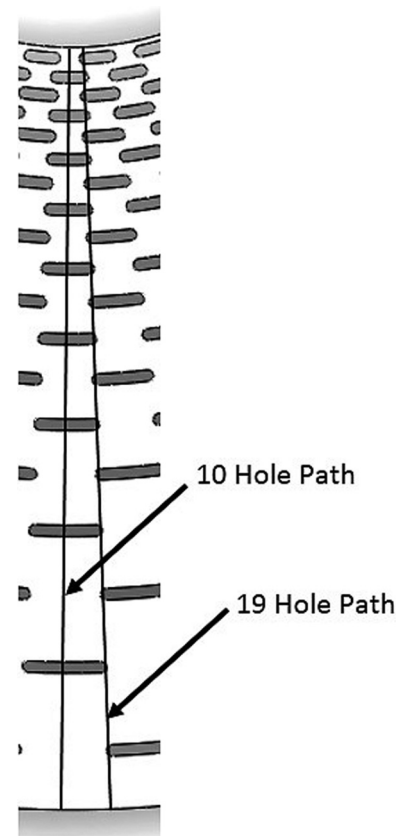
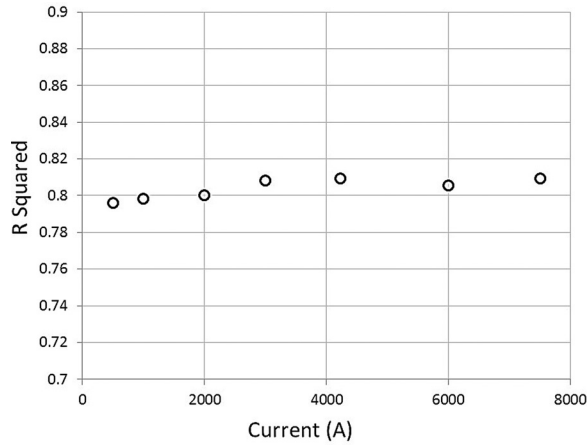


Fig. 6 Radial line elements intersecting 19 and 10 holes

(shown in Fig. 6), the analytic prediction exceeds the trend of the FEA data near the inner radius of the disk. Figure 5, however, reveals that along a radial line element which spans 19 cooling channels (Fig. 6), the analytic prediction is below the FEA data. These patterned discrepancies occur because the analytic prediction given by Eq. (11) assumes that the joule heating profile does not vary circumferentially. The resistance along the 19 hole line element and consequently the volumetric joule heating is higher because of the reduced cross-sectional area. The ten hole line element has a greater cross-sectional area, and thus a lower joule heating profile. Equation (11) does not take into account these



**Fig. 7** *R* squared of the joule heat profile (evaluated with Eq. on a logarithmic scale) versus applied current

variations in cross-sectional area. This explains why the analytic prediction appears to attain values that constitute an average of the two cases.

Note that the sinusoidal appearance of the joule heating profile in Fig. 4 reflects the current flow around the cooling holes. (The peaks of the heating profile correspond to the locations of cooling holes.) The profile of the 19 hole path has a less pronounced sinusoidal shape because there are more cooling channels interrupting the 19 hole path. Thus, the 19 hole profile varies on a smaller scale. The profiles are created with the same number of data points for comparison.

If the FEA joule heating profiles for the ten hole and 19 hole paths are combined into a single logarithmic plot, the *R* squared of Eq. (11) is found to be approximately 0.81. Figure 7 shows the *R* squared values of Eq. (11) compared with FEA data for eight different applied currents. *R* squared or the coefficient of determination quantifies the variability of data with respect to a model. Unity indicates the minimum possible variability, and zero corresponds to maximum variability [8]. *R* squared is calculated with:  $R^2 = 1 - (\sum_{l=0}^{l=m_{data}} (x_{l_{data}} - x_{l_{fit}})^2 / \sum_{l=0}^{l=m_{data}} (x_{l_{data}} - \bar{x}_{data})^2)$ , where  $x_{l_{data}}$  is the *l*th data point,  $x_{l_{fit}}$  is the *l*th point on the fit line,  $m_{data}$  is the total number of data points, and  $\bar{x}_{data}$  is the mean of the data points.

#### 4 Elemental Joule Heating

Equation (11) can now be used to find cooling channel designs that establish a manageable temperature profile throughout the coil. In the 1960s, Montgomery derived a method for placing cooling holes [6], but his methods are based on empirically determined equations that only apply to magnets with circular cooling channels. The specific solution obtained below applies only to the elongated cooling channel design; however, it can be generalized to arbitrary cooling hole shapes, provided Eqs. (4)–(11) are derived for such shapes.

The general methodology for designing the cooling system is to divide the coil into individual elements with a cooling channel running through the center of each and ensure that a safe thermal equilibrium is achieved for each element.

To find the heat generated within each element, Eq. (11) must be integrated over the volume of the element. The general formula for total joule heating in an element is given by

$$W_{el} = \int_V w_v(r) dV \quad (12)$$

Inserting Eq. (11) yields the general expression for the total heating in a single element

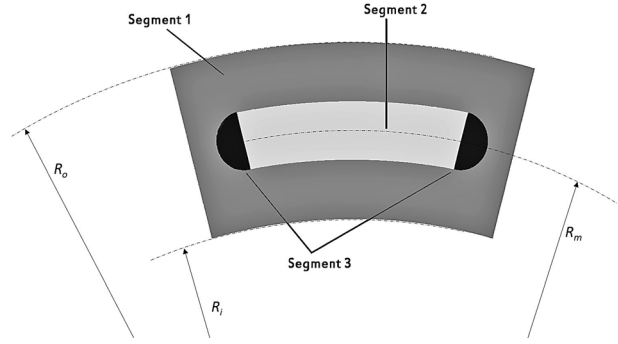


**Fig. 8** Segment divisions within one polar rectangle lattice cell

$$W_{el} = \int_V \frac{W}{2\pi N_T \alpha_T t \left[ \left( 1 - \frac{n N_R d \phi}{2\pi(a_2 - a_1)} \right) \ln \left( \frac{a_2}{a_1} \right) - \frac{n N_R d^2}{8 a_2 a_1} \right]} \frac{1}{r^2} dV \quad (13)$$

For simplicity, a constant  $C_0$  can be defined as

$$C_0 = \frac{W}{2\pi N_T \alpha_T t \left[ \left( 1 - \frac{n N_R d \phi}{2\pi(a_2 - a_1)} \right) \ln \left( \frac{a_2}{a_1} \right) - \frac{n N_R d^2}{8 a_2 a_1} \right]} \quad (14)$$

Hence, the integral becomes

$$W_{el} = C_0 \int_V \frac{1}{r^2} dV \quad (15)$$

To evaluate this integral, it is most convenient to divide the surface of the element into three area segments (refer to Fig. 8) where segment 1 is the total region of the polar rectangle. The total joule heating in the element is given by

$$W_{el} = W_1 - W_2 - W_3 \quad (16)$$

The joule heating in segment 1 is

$$W_1 = C_0 \int_0^{N_T \alpha_T t} \int_0^{\frac{2\pi}{n}} \int_{R_i}^{R_o} \frac{1}{r} dr d\theta dz \quad (17)$$

This integral becomes

$$W_1 = 2\pi C_0 N_T \alpha_T t \ln \left( \frac{R_o}{R_i} \right) \frac{1}{n} \quad (18)$$

where  $2\pi/n$  is the angle span of each element (assuming that all the elements have equal angle spans as seen in Fig. 3),  $R_o$  is the outer radius of the element, and  $R_i$  is the inner radius.

The joule heating in segment 2 is

$$W_2 = C_0 \int_0^{N_T \alpha_T t} \int_0^{\phi} \int_{R_m-d/2}^{R_m+d/2} \frac{1}{r} dr d\theta dz \quad (19)$$

$$= C_0 \phi N_T \alpha_T t \ln \left( \frac{R_m + \frac{d}{2}}{R_m - \frac{d}{2}} \right) \quad (20)$$

where  $R_m$  is defined as the radial placement of the middle of the cooling channel.



Finally, the joule heating must be found in the semicircular ends. The complete derivation of the expression below is given in the Appendix. (To check that the following integral correctly models the circular region of segment 3, replace the integrand with a “1” and compare this with the expression for the volume of a circular cylinder.)

$$W_3 = 2C_0 \sum_{i=1}^k \left[ \int_0^{N_T \alpha_T t} \int_0^{\gamma_i} \int_{R_m + \frac{2k}{d(k-2i)}}^{R_m + \frac{d(k-2i+2)}{2k}} \frac{1}{r} dr d\theta dz \right] \quad (21)$$

$$= 2C_0 N_T \alpha_T t \sum_{i=1}^k \left[ \gamma_i \ln \left( \frac{R_m + \frac{d(k-2i+2)}{2k}}{R_m + \frac{d(k-2i)}{2k}} \right) \right]$$

where  $\gamma_i$  is given by

$$\gamma_i = \arccos \left[ \frac{\left( R_m + \frac{d(k-2i+1)}{2k} \right)^2 + R_m^2 - \frac{d^2}{4}}{2R_m \left( R_m + \frac{d(k-2i+1)}{2k} \right)} \right] \quad (22)$$

Typically, Eq. (21) converges to five significant figures after  $k = 3000$ , and to three significant figures after  $k = 200$ .

## 5 Convective Heat Transfer

In order to design the magnet such that a predictable thermal equilibrium is achieved, Eq. (16) must be set equal to the convective heat transfer term at the cooling hole boundaries. Unlike joule heating, the governing equations for convection are generally determined by empirical analyses, the bulk of which only take circular duct geometry into account. Thus, expressions for convective heat transfer in Bitter magnet cooling channels are often debated [7].

The general expression for convective heat transfer is

$$q = h A_s (T_s - T_f) \quad (23)$$

where  $A_s$  is the surface area exposed to the fluid flow,  $T_s$  is the temperature of the solid surface, and  $T_f$  is the fluid temperature. Thus, determining  $q$  is a matter of finding an appropriate expression for  $h$ , the heat transfer coefficient.

Typically, it is prudent to ensure that the flow of cooling water is sufficiently high to induce turbulent flow within the cooling channels [7]. Turbulent flow is desirable because heat transfer is more efficient, and because analytic equations for the heat transfer coefficients are more readily obtainable. Thus, if turbulent flow conditions can be achieved, the cooling capacity is improved and the heat transfer is more predictable. The equation we use to find  $h$  was originally derived by Dittus and Boelter and is suitable for predicting heat transfer in flow with Reynolds numbers greater than 2300 and less than  $1.2 \times 10^5$  in smooth circular pipes [9]. The expression is suitable for generalization to noncircular ducts as well [10]. A very similar expression was used by Francis Bitter to model water cooling in 1936 [3]. The Dittus–Boelter expression for circular pipes is given by

$$\left( \frac{hD}{K_b} \right) = 0.023 \left( \frac{Dvp}{\mu_b} \right)^{0.8} \left( \frac{c_p \mu_b}{K_b} \right)^{0.4} \quad (24)$$

where  $D$  is the diameter of the duct,  $K$  is the thermal conductivity of water,  $v$  is the velocity,  $p$  is the density of water,  $c_p$  is the specific heat of water at constant pressure, and  $\mu$  is the dynamic viscosity. The subscript,  $b$ , indicates that the variable is evaluated at the bulk mean temperature of the fluid. Solving for  $h$  yields

$$h = 0.023 D^{-0.2} K_b^{0.6} (vp)^{0.8} \left( \frac{c_p}{\mu_b} \right)^{0.4} \quad (25)$$

Kays suggests that for turbulent flow in rounded noncircular pipe geometries, it is reasonable and, in fact, accurate to use the same heat transfer equations, but with hydraulic diameter instead of diameter [11]. Hydraulic diameter is given by

$$D_h = \frac{4A}{P} \quad (26)$$

where  $A$  is the area of the channel, and  $P$  is the perimeter of the channel exposed to fluid flow. Hence, the equation for convective heat transfer in elongated holes is given by

$$q = 0.023 D_h^{-0.2} K_b^{0.6} (vp)^{0.8} \left( \frac{c_p}{\mu_b} \right)^{0.4} A_s (T_s - T_f) \quad (27)$$

Another problem associated with the convective heat transfer is defining the water velocity in each cooling channel. Our magnet design assumes a constant pressure head over all the holes as well as negligible inlet pressure losses (we intend to accomplish this with chamfered or rounded inlets). Therefore, the fluid velocity in the cooling channels is ideally only a function of the inlet–outlet pressure difference (constant for all holes), the roughness of the channel, and the geometry of the channel. For turbulent flow, the Darcy–Weisbach equation is used to determine pressure drop [12]

$$\Delta P = f \frac{(2b)p v^2}{2D_h} = f \frac{bp v^2}{D_h} \quad (28)$$

where  $f$  is the Darcy friction factor, and  $2b$  is the length of the cooling channel. Typically, the Colebrook equation is used to model the Darcy friction factor for turbulent flow in circular and noncircular ducts [13]. This equation, however, requires an iterative process to solve for  $f$ . Thus, an accurate approximation of the Colebrook equation formulated by Swamee and Jain (which is cited in Ref. 14) is used to simplify calculations

$$f = 0.25 \left[ \log_{10} \left( \frac{\varepsilon}{3.7 D_h} + 5.74 \left( \frac{\mu_b}{D_h p v} \right)^{0.9} \right) \right]^{-2} \quad (29)$$

where  $\varepsilon$  is an empirically determined roughness factor. And so, the equation for pressure drop becomes

$$\Delta P = 0.25 \left[ \log_{10} \left( \frac{\varepsilon}{3.7 D_h} + 5.74 \left( \frac{\mu}{D_h p v} \right)^{0.9} \right) \right]^{-2} \frac{bp v^2}{D_h} \quad (30)$$

A simple iterative root-finding program can be used to solve for the water velocity,  $v$ . This provides sufficient information to determine the cooling capacity of each channel given a predetermined pressure head.

## 6 Integrated Design Method

The expressions above can now be used to obtain a thermally acceptable cooling channel design. We deem a design to be acceptable if analytic calculations and FEA show that the following conditions are met: (i) The temperature of the water at the cooling channel outlets is sufficiently below the boiling point of water to satisfy a predetermined factor of safety. (ii) The peak temperature within the magnet does not exceed a predetermined maximum. (iii) The requisite pressure head and flow rate are feasible given limitations inherent to the pump and the other elements of the hydraulic system. (iv) The peak mechanical stresses within the magnet and support struts do not exceed predetermined maxima.

The specific design method currently in use at the UMBC Dusty Plasma Laboratory follows the sequence described below. Nested and single coil designs are considered in order to obtain a spectrum of designs from which we can choose the most economically feasible.

- (1) Formulations are derived from Maxwell's equations to provide the magnetic field of the proposed solenoid magnet design. The magnetic field equation gives the field along the axis of the magnet for a certain number of nested solenoids, inner radius, current, number of magnetic turns, and length of the solenoid. This equation can also be modified to accommodate a split magnetic coil design [4].

The problem is to optimize the magnet's design parameters to minimize power and produce a fixed magnitude of field. This is a nonlinear constrained global optimization problem where the solutions of the nested magnetic solenoid design can be presented on a Pareto Frontier [15]. The choice of the number of nested solenoid coils versus the total power requirement is then based on engineering fabrication, and cost. To obtain solutions, a differential evolution optimization method is used which is a variation of the common genetic algorithm. Minimizing power in the magnet is the objective function, and the main constraint is the magnetic field strength at the center of the experimental volume, where dusty plasma experiments will take place. The number of turns, length, inner and outer radii, separation distances, copper filling factor, and current are all the design variables. Many of these design variables have imposed constraints from both design and feasibility standpoints. Optimization solutions are produced with Mathematica [16] and then tabulated for comparisons. Details of the electromagnetic calculations and optimization will be presented elsewhere.

- (2) After the first iteration of electromagnetic optimization is completed, there is sufficient information to design an initial water cooling system.

The innermost ring of cooling holes is designed using the equations and methods described in Secs. 4 and 5. This ring is designed such that the water pressure required to reach thermal equilibrium is less than the maximum achievable pressure. It is also important that the flow velocity produced by the pressure is sufficiently large to establish turbulent flow conditions within the cooling passages.

All other rings are designed such that thermal equilibrium is attained given the pressure head determined for the innermost ring. Because of the temperature gradient that arises between adjacent cooling holes, it is important that the holes be tightly packed. Inevitably, the field of cooling holes initially produced by this process will not fit perfectly into the space of the Bitter disks. Thus, various design parameters should be modified until the outer radius of the outermost element equals the outer radius of the coil,  $a_2$ . In our analysis, the thermal interactions between adjacent nested coils are not considered.

- (3) The peak mechanical stress within the coil is checked with FEA software. If this stress exceeds the maximum stress prescribed by the factor of safety, the cooling hole placement and disk thickness are modified until the factor of safety is met.

After reiterating the above steps until design convergence is attained, the resulting coils will have the desired field, a uniform temperature at all the cooling channel walls (unless a variable temperature parameter is prescribed), and an acceptable mechanical support structure. Figure 9 shows an FEA rendering of the temperature profile of a Bitter disk with 19 cooling channel rings, given 4200 A (the disk is shown in Fig. 1). The above described thermal design method was used to place all the cooling channels and to determine the required convective heat

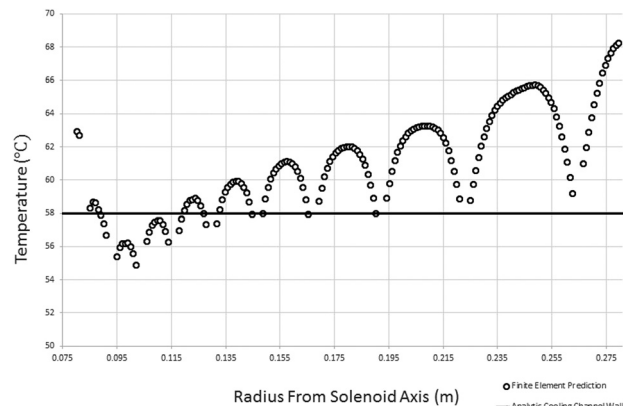


Fig. 9 Temperature profile of a copper disk given 4200 A-10 hole path

transfer components. The width of the cooling holes (the variable given as " $d$ " in the above equations) was set to be 3 mm, and the sweep angle of the cooling holes (given as " $\phi$ " above) was set to 4.5 deg. With a water temperature of 5 °C, the temperature at the cooling channel walls was predicted by the analytic formulae to be 58 °C. The minimum Reynolds number required to achieve this cooling was calculated to be 5500 (channels at the innermost ring of cooling channels have the smallest hydraulic diameter and consequently the minimum Reynolds number). The temperature profile shown in Fig. 9 reveals that the cooling channel walls (indicated in the graph by sharp drops in the temperature profile) reach temperatures within  $\sim 1.5\%$  of the predicted 331 K. Structural FEA results revealed that the peak equivalent stress in this magnet design is approximately 60 MPa which is well below 345 MPa, the yield strength of cold worked oxygen-free copper [17]. Oxygen-free copper such as C10100 is considered because of the high electrical conductivity of this material and because the case studies we have explored thus far have not indicated a need for higher strength conductors.

## 7 Conclusion

The above described methods should be capable of constructing thermally viable Bitter magnets without heavy reliance on FEA. Note that the expressions associated with convective heat transfer must be given a high factor of safety simply because of their empirical, application-specific nature. It is undeniably more accurate to empirically determine the constants and relations of fluid mechanics.

The purely analytic thermal design method we are employing has allowed us to rapidly explore the feasibility of numerous unique design concepts. After the requisite power and size parameters are generated, a program employing the design method described above can create as many as 15 different cooling channel designs in less than an hour. From these designs, one or more optimum solutions can be selected. Analytic methods cannot be as detailed or accurate as FEA, but they represent a legitimate option for low powered magnet designers seeking a time efficient design scheme. The method we present was originally conceived to create the thermal system of our 16 cm bore 10 T magnet; however, as seen in Fig. 7, the analytic joule heating equation (Eq. (11)) predicts the heating profiles at a wide range of current densities. Our analytic approach has given us the ability to quickly obtain a breadth of knowledge regarding feasible designs. Additionally, it has proved to be sufficiently accurate to give us confidence that our final design solution is optimal.

## Acknowledgment

We would like to acknowledge the Special Research Assistantship/Initiative Support and the Department of Mechanical Engineering at UMBC for supporting this research.

## Appendix: Joule Heat Integrated Over an Offset Circular Section

The following is a derivation of the method used to integrate volumetric joule heating over a circular section that is offset from the center axis. The resulting expression is used to find the total joule heat generated in the semicircular ends or segment 3 of the elongated cooling passages (see Fig. 8). This joule heat generation can then be used to find total elemental joule heating (see Eq. (16)).

In order to integrate volumetric joule heating (Eq. (12)) over segment 3, the circular region is split into several polar rectangles of equal radial thickness (as seen in Fig. 10). To better approximate the area, the rectangles are placed so that the middle line intersects the circle. The joule heating in the  $i$ th segment is given by the following integral. Since the joule heating profile does not vary with  $\theta$ , it is symmetric with respect to the vertical axis. Thus, heating in only half the region (left or right) needs to be calculated. The heat generation in the total region is twice this value

$$W_i = 2 C_0 \int_0^{N_T \alpha_T t} \int_0^{\gamma_i} \int_{r_{ii}}^{r_{oi}} \frac{1}{r^2} r dr d\theta dz \quad (A1)$$

All that remains to evaluate this integral is to determine the values of the angle,  $\gamma$  (in radians); the inner segment radius,  $r_i$ ; and the outer segment radius,  $r_o$ , which correspond to the  $i$ th segment. The thickness (radial extent) of a single segment in a circular region divided into  $k$  segments is given by

$$r_{oi} - r_{ii} = \frac{d}{k} \quad (A2)$$

Thus, if the segments are sequenced starting with the outermost segment (i.e., the segment farthest from the centerline is the first), the outer and inner radii (respectively) of the  $i$ th segment can be defined as follows:

$$r_{oi} = R_m + \frac{d}{2} - \frac{d(i-1)}{k} = R_m + \frac{d[k-2(i-1)]}{2k} \quad (A3)$$

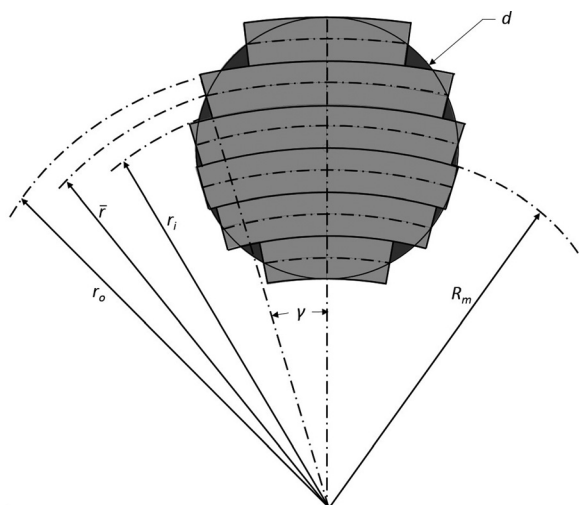


Fig. 10 Segment 3 divided into approximating sections

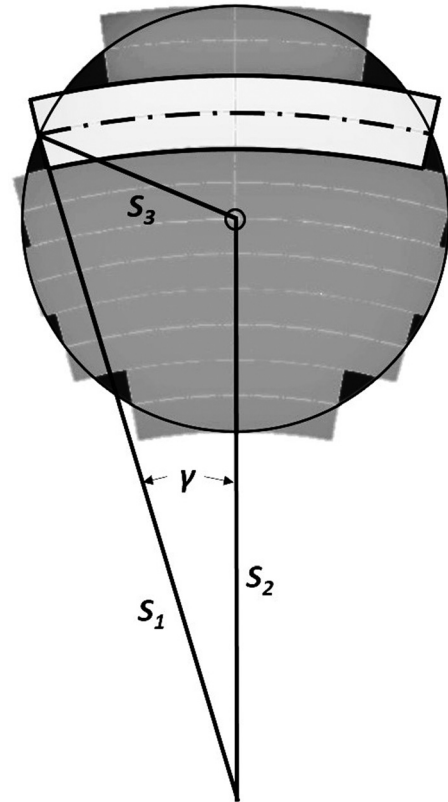


Fig. 11 Parameters of the  $i$ th segment (the lightly shaded region denotes a representation of the  $i$ th segment)

$$r_{ii} = R_m + \frac{d}{2} - \frac{d(i-1)}{k} - \frac{d}{k} = R_m + \frac{d(k-2i)}{2k} \quad (A4)$$

The law of cosines can be used to determine  $\gamma_i$ . Given three sides  $S_1$ ,  $S_2$ , and  $S_3$  (see Fig. 11), the expression for  $\gamma_i$  is given by

$$\gamma_i = \arccos\left(\frac{S_1^2 + S_2^2 - S_3^2}{2 S_1 S_2}\right) \quad (A5)$$

where

$$S_1 = R_m + \frac{d}{2} - \frac{d(i-1)}{k} - \frac{d}{2k} = R_m + \frac{d(k-2i+1)}{2k} \quad (A6)$$

$$S_2 = R_m \quad (A7)$$

$$S_3 = \frac{d}{2} \quad (A8)$$

Thus, Eq. (A5) becomes

$$\gamma_i = \arccos\left[\frac{\left(R_m + \frac{d(k-2i+1)}{2k}\right)^2 + R_m^2 - \frac{d^2}{4}}{2 R_m \left(R_m + \frac{d(k-2i+1)}{2k}\right)}\right] \quad (22)$$

Inserting Eqs. (A3) and (A4) into Eq. (A1) yields the expression for joule heating in the  $i$ th segment

$$W_i = 2 C_0 \int_0^{N_T \alpha_T t} \int_0^{\gamma_i} \int_{R_m + \frac{d(k-2i)}{2k}}^{R_m + \frac{d(k-2i+2)}{2k}} \frac{1}{r^2} r dr d\theta dz \quad (A9)$$



Equation (21) can now be obtained by summing the joule heating in all  $k$  approximating segments

$$W_3 = 2C_0 \sum_{i=1}^k \left[ \int_0^{N_T \alpha_T t} \int_0^{\gamma_i} \int_{R_m + \frac{d(k-2i)}{2k}}^{R_m + \frac{d(k-2i+2)}{2k}} \frac{1}{r^2} r dr d\theta dz \right] \quad (21)$$

$$= 2C_0 N_T \alpha_T t \sum_{i=1}^k \left[ \gamma_i \ln \left( \frac{R_m + \frac{d(k-2i+2)}{2k}}{R_m + \frac{d(k-2i)}{2k}} \right) \right]$$

## References

- [1] Dixon, I., Bird, M. D., and Bole, S., 2002, "End Effects in the NHMFL 45 T Hybrid Resistive Insert," *IEEE Trans. Appl. Supercond.*, **12**(1), pp. 452–455.
- [2] Brechna, H., and Montgomery, D. B., 1962, "A High Performance D.C. Magnet Utilizing Axial Cooled Disks," *NML*, **62**(1), pp. 1–44.
- [3] Bitter, F., 1936, "Design of Powerful Electromagnets: Part II—The Magnetizing Coil," *Rev. Sci. Instrum.*, **7**(12), pp. 482–488.
- [4] Bird, M. D., Bole, S., Eyssa, Y. M., Gao, B. J., and Schneider-Muntau, H. J., 1996, "Design of a Poly-Bitter Magnet at the NHMFL," *IEEE Trans. Magn.*, **32**(4), pp. 2542–2545.
- [5] Gao, B., Schneider-Muntau, H., Eyssa, Y., and Bird, M., 1996, "A New Concept in Bitter Disk Design," *IEEE Trans. Magn.*, **32**(4), pp. 2503–2506.
- [6] Montgomery, D. B., 1969, *Solenoid Magnet Design: The Magnetic and Mechanical Aspects of Resistive and Superconducting Systems*, Wiley-Interscience, New York, Chap. 4.
- [7] Bird, M. D., 2004, "Resistive Magnet Technology for Hybrid Inserts," *Supercond. Sci. Technol.*, **17**(8), pp. R19–R33.
- [8] Hicks, C. R., and Turner, K. V., 1999, *Fundamental Concepts in the Design of Experiments*, 5th ed., Oxford University Press, New York, Chap. 3.
- [9] Sukhatme, S. P., 2005, *A Textbook on Heat Transfer*, 4th ed., Universities Press, Hyderabad, India, Chap. 5.
- [10] Chapman, A. J., 1984, *Heat Transfer*, 4th ed., Macmillian, New York, Chap. 8.
- [11] Kays, W. M., and Crawford, M. E., 1993, *Convective Heat and Mass Transfer*, 3rd ed., McGraw-Hill, New York, Chap. 14.
- [12] Munson, B. R., Okiishi, T. H., Huebsch, W. W., and Rothmayer, A. P., 2013, *Fundamentals of Fluid Mechanics*, 7th ed., Wiley, New York, Chap. 8.
- [13] Granger, R. A., 1985, *Fluid Mechanics*, CBS College Publishing, New York, Chap. 10.
- [14] Babatola, J., Oguntuase, A., Oke, I., and Ogedengbe, M., 2008, "An Evaluation of Frictional Factors in Pipe Network Analysis Using Statistical Methods," *Environ. Eng. Sci.*, **25**(4), pp. 539–547.
- [15] Scap, D., Hoić, M., and Jokzć, A., 2013, "Determination of the Pareto Frontier for Multi-Objective Optimization Problem," *Trans. FAMENA*, **37**(2), pp. 15–28.
- [16] Wolfram, S., 2012, "Mathematica 9."
- [17] Brady, G. S., and Clauser, H. R., 1991, *Materials Handbook Part 1*, 13th ed., McGraw-Hill, New York.